Applied Catalysis B: Environmental 200 (2017) 578–584

Contents lists available at ScienceDirect

Applied Catalysis B: Environmental

journal homepage: www.elsevier.com/locate/apcatb

Nickel nanoparticles coated with graphene layers as efficient co-catalyst for photocatalytic hydrogen evolution

Li Jun Fang[a,b,1], Xue Lu Wang[a,1], Yu Hang Li[a,1], Peng Fei Liu[a], Yu Lei Wang[a], Hui Dan Zeng[b], Hua Gui Yang[a,*]

[a] Department Key Laboratory for Ultrafine Materials of Ministry of Education, School of Materials Science and Engineering, East China University of Science and Technology, 130 Meilong Road, Shanghai 200237, China
[b] Department School of Materials Science and Engineering, East China University of Science and Technology, 130 Meilong Road, Shanghai, 200237, China

ARTICLE INFO

Article history:
Received 27 March 2016
Received in revised form 28 June 2016
Accepted 19 July 2016
Available online 19 July 2016

Keywords:
Photocatalysis
Co-catalyst
Hydrogen
Ni@C
Graphene layers

ABSTRACT

Metallic nickel nanoparticles well dispersed in graphitized carbon matrix (Ni@C) by pyrolysis of metal-organic frameworks and leaching treatment of hydrochloric acid could greatly enhance the photocatalytic activity of g-C_3N_4 under visible light irradiation. For 2.0 wt% Ni@C/g-C_3N_4, the average hydrogen evolution rate is 2.15 mmol h^{-1} g^{-1}, which is around 88 times higher than that of pure g-C_3N_4, and even better than that of platinum-loaded g-C_3N_4. The remarkably improved photocatalytic activities through loading Ni@C can be attributed to the cooperative work of Ni nanoparticles and graphene layers, which facilitate the separation of photo-generated carriers and suppress the recombination of the electron-hole pairs. In addition, the hollow onion-like structure can restrain the formation of Ni-hydrogen bonds which modulates desorption of hydrogen. Our studies may open up a promising strategy to design economical noble-metal-free co-catalysts for efficient solar energy conversion.

1. Introduction

As one of the most appealing approaches to solve the global energy crisis and environmental pollution, hydrogen (H_2) produced through sunlight-driven water splitting has attracted increasing attention since the pioneering study in 1970s when Fujishima and Honda first discovered the phenomenon of photocatalysis water into H_2 [1,2]. Although tremendous progress has been achieved, low light utilization efficiency and instability of numerous photocatalysts still set hurdles for real applications [3]. Hence, exploring efficient and endurable photocatalysts for H_2 evolution from water still remains a great challenge. As a low-cost, stable, metal-free, nontoxicity and visible-light-active photocatalyst, the typical two-dimensional layered material, polymeric graphitic carbon nitride (g-C_3N_4) has drawn multitudinous research enthusiasm since it was explored by Wang et al. in 2009 [4,5]. As a promising material, g-C_3N_4 can be applied in the potential fields of environmental remediation, hydrogen or oxygen evolution from splitting water, carbon dioxide reduction, hydrogen storage, lithium batteries, solar-photovoltaic energy, and as an electrode material for super capacitors [6]. The ointment is that the solar energy conversion efficiency of pristine g-C_3N_4 is low because of ultrafast recombination of photo-induced charges, small surface area and poor mass diffusion [6,7]. In order to overcome these intrinsic drawbacks of g-C_3N_4, several methods have been employed, such as doping with metal or nonmetal species [8–10], copolymerization [11], morphology optimization [12] and surface modification [13]. Loading co-catalysts which can promote the separation of photo-generated electron-hole pairs and offer the active sites for H_2 or oxygen generation is one of the most effective strategies to improve the catalytic efficiency of g-C_3N_4 [14]. Among them, platinum (Pt) and other noble metals are the most common co-catalysts [5,15]. However, in view of its high price and scare supply, it is still urgently needed to explore noble-metal-free co-catalysts. To date, intensive efforts have been made to modify the catalytic behavior of earth-abundant transition metals, such as Ni, Mo, Co [5,16]. However, the poor chemical stability and low photoactivity of these substitutions retard their large-scale applications [17]. Among them, many Ni-based co-catalysts, such as metallic Ni, sulfides, phosphides, oxides hydroxides, hydrogenases, as well as molecular complexes, have already exhibited the promising alternative candidate as the H_2-evolution co-catalysts [18]. Recently, metallic Ni has been proved to serve as the H_2 evolution site and maintaining the metallicity of these co-catalysts is favorable to produce H_2 from water [19,20].

* Corresponding author.
E-mail address: hgyang@ecust.edu.cn (H.G. Yang).
[1] These authors contributed equally to this work.

http://dx.doi.org/10.1016/j.apcatb.2016.07.033
0926-3373/

Unfortunately, according to the principle of Sabatier, the existence of strong bonds between transition metals and H_2 leads to a deterioration of catalyst performances [20].

Graphitic carbon materials with good thermal and chemical stabilities have attracted much interest for many potential applications in recent years, especially in the field of tackling down the energy and environmental problems [21]. Photocatalysts can further increase the optical absorption property and providing more active adsorption sites for photocatalytic reactions with the aid of graphene. Since the excellent electrical conductivity property, graphene could accelerate the delivering of the photo-induced carriers to the active sites, resulting in a reduction in charge combination when introduced into photocatalyst. Due to the same carbon element, graphitic carbon materials can form interfacial contact with g-C_3N_4 which enhanced visible light intensities toward a longer wavelength region [22]. Carbonization of metal-organic frameworks (MOFs) without the need for complicated processes is a facility method to prepare graphitic carbon materials [23]. In previous works, our group has synthesized Ni nanoparticles wrapped up by graphene layers with hollow onion-like structure through thermal decomposition of MOFs and leaching treatment of hydrochloric acid (HCl). The obtained Ni@C catalyst was used in electrocatalysis of the H_2 evolution reaction [24]. Inspired by its impressive efficiency, we further proved that Ni@C can also act as a high-efficiency co-catalyst for photocatalytic H_2 evolution via loading it on the surface of g-C_3N_4. Graphitized carbon shells have played an important role in the catalytic process. Firstly, owing to the electronic conductivity of carbon materials, the photo-generated electrons can be trapped by the active centers quickly through the outer shell [24,25]. Secondly, the presence of the protective shell can suppress the formation of metal-H_2 bonds on the surface of transition metals which is conducive to the desorption of H_2 [16,20,26]. Additionally, graphene layers can act as a good barrier for O_2 diffusion and the hollow onion-like structure could also inhibit the undesirable reverse reaction [26,27].

Herein, g-C_3N_4 has been chosen as the host photocatalyst and under optimum conditions, Ni@C/g-C_3N_4 exhibits an excellent H_2 evolution reaction (HER) property as high as $\sim$2151.4 μmol h^{-1} g^{-1} ($\lambda > 420$ nm), which is 88.3 times higher than that of raw g-C_3N_4, and even higher than that of 2.0 wt% Pt/g-C_3N_4 sample. To the best of our knowledge, few researches of carbonized MOFs have centered on the field of photocatalysis, and this work may open up new insights into the design of co-catalysts.

2. Experimental

2.1. Synthesis of Ni@C/g-C_3N_4

The pristine g-C_3N_4 powder was synthesized by a slight modified thermal polymerization method according to the literature [28]. Typically, 10 g urea was heated in a 30 mL alumina crucible with a cover in a muffle furnace in static air. The calcination parameter was set as follows: from room temperature to 500 °C at a heating rate of 5 °C min^{-1}; it was finally maintained at 500 °C for 2 h. The light yellow g-C_3N_4 was obtained after cooling down to room temperature. Then, the resultant agglomerates were mashed into powder with a glass stirring rod and collected for the further use.

Ni@C was synthetized according to our previous work [24]. Ni@C/g-C_3N_4 samples were prepared by conventional wet impregnation method [29]. Briefly, 0.1 g g-C_3N_4 and an appropriate amount of Ni@C were added into alumina crucible containing 5 mL ethanol. Subsequently, the reactant solution was placed in an ultrasonic bath for 30 min in order to get homogeneously dispersing suspension. Then, the slurry was stirred at 80 °C in water bath until the liquid was evaporated. Finally, the mixture was calcined at 150 °C for 2 h at a heating rate of 2 °C min^{-1}. After the reaction cooling down, the as-prepared specimens were used directly for photocatalytic reactions without further processing. For comparison, freshly-prepared g-C_3N_4 was also prepared via a similar procedure in the absence of Ni@C.

2.2. Photocatalyst characterization

The morphology and structures of the as-prepared samples were observed on scanning electron microscopy (SEM, HITACHI S4800). Besides the morphology and structures, lattice fringe and selected area electron diffraction (SAED) were analyzed by transmission electron microscopy (TEM, JEM 2100, 200 kV). X-ray diffraction (XRD, D/MAX 2550 VB/PC) was employed to study the structures of the powder samples. Raman spectrum was obtained on a Rennishaw InVia spectrometer with an excitation wavelength of 785 nm. Infrared transmission patterns were measured by Fourier transform infrared (FTIR) spectrophotometer Spectrum (Nicolet). The ratios of carbon and nitrogen contents were obtained using an elemental analyzer (vario EL α, Elementar Analysensyteme, Germany). The binding energies of surface elements were investigated by X-ray photoelectron spectroscopy (XPS, Kratos Axis Ultra DLD, all binding energies were referenced to the C 1s peak, 284.6 eV). The Ni contents in the samples both before and after irradiation were determined by inductively coupled plasma atomic emission spectroscopy (ICP-AES, Varian 710ES). Ultraviolet-visible (UV–vis) diffuse reflection spectra of the samples was obtained using a UV–vis spectrometer (CARY 500). The photoluminescence (PL) spectra was employed to test the recombination rates of electron-hole pairs by an Edinburgh Instruments (FLSP 920) system operated at room temperature.

2.3. Photoelectrochemical analysis

The standard three-electrode system was used to test the transient photocurrent response and electrochemical impedance spectroscopy (EIS) using a Pt foil and Ag/AgCl as counter and reference electrodes respectively. And 0.2 M Na_2SO_4 aqueous solution containing 10 vol.% triethanolamine (TEOA) was chosen as the supporting electrolyte. The working electrode was prepared as follows: 10 mg of the catalyst powder was dispersed into 50 μL nafion and 200 μL DMF solution by ultrasound. And then 20 μL slurry was spread on a 1.0 × 2.5 cm fluorine-doped tin-oxide (FTO) glass substrate whose side part was previously protected by Scotch tape, with an active area of approximately 1.0 cm^2. The resulting electrodes were dried in the air. The measurements were performed under one sun condition using a solar light simulator (Oriel, 91160, AM 1.5 globe). And the power of the simulated light was adjusted to 100 mW cm^{-2}. The EIS experiments were operatured on a CH Instruments Electrochemical Workstation under 1.0 V vs. Ag/AgCl.

2.4. Photocatalytic activity measurements

The solar-driven H_2 productions from water experiments were conducted to test the activities of the photocatalysts. Typically, 30 mg photocatalyst was dispersed in 80 mL deionized water and 20 mL TEOA functioning as a sacrificial electron donor. For the contrastive sample, 2.0 wt% of Pt was loaded on the surface of g-C_3N_4 through the above method and H_2PtCl_6 was chosen as the starting material. The catalytic reaction was performed in a Pyrex glass cylinder of about 200 mL with a piece of optically polished quartz glass as its top cover which was connected to a glass closed gas system. The photocatalytic system was irradiated with 300 W Xe arc lamp equipped with an ultraviolet cutoff filter to provide visible light with $\lambda > 420$ nm. In order to exclude the impact of air

and conducive to the spread of the evolved gas, the system was evacuated thoroughly several times by vacuum pump before illumination. Ultrasound before the reaction and magnetic stir during the reaction ensured the uniformity of the reaction solution. The amount of evolved H_2 was analyzed by an online gas chromatograph (GC2014C, Shimadzu, with argon as a carrier gas) equipped with a thermal conductivity detector (TCD) and molecular sieve 5-Å column. The H_2 content was monitored every 30 min in order to determine the production rate.

The apparent quantum yield (QY, %) for H_2 evolution was estimated in term of the following equation with a 420 nm band-pass filter [9]:

$$QY(\%) = Ne/Np = 2N_{H_2}/N_p \quad (1)$$

Here Ne represents for the number of reacted electrons, N_{H_2} stands for the number of evolved H_2 molecules and Np is the number of incident photons.

3. Results and discussion

Scanning electron microscopy (SEM) and transmission electron microscopy (TEM) were used to investigate the morphology and microstructures of pristine g-C_3N_4 and 2.0 wt% Ni@C/g-C_3N_4. Obviously, the homogeneous dispersion of Ni@C grains on g-C_3N_4 surface is evidenced by SEM and TEM images (Fig. S1b and Fig. 1a), which was further confirmed by the elemental mapping (Fig. S2). The SEM images (Fig. S1) displayed the typical two-dimensional layered silk like structure, indicating that loading Ni@C has no effect on the stratiform morphology of g-C_3N_4 [30]. Meanwhile, the detailed local structures of Ni@C anchored on g-C_3N_4 were studied by HR-TEM. The TEM image of Ni@C nanoparticles was insetted in Fig. 1a. As shown in Fig. 1b, the metallic Ni nanoparticles are encapsulated well in several graphene layers. The average diameter of dark Ni@C is about 10 nm and the lattice fringe with d-spacing of 2.04 Å can be ascribed to the (111) plane of cubic phase Ni [24]. The blurry and incomplete lattice fringes in the outer boundary could be graphitized carbon layers and the (002) d-spacing (~3.45 Å) of the graphitic carbon layers coincide with our previous report well [24]. No apparent diffraction rings of Ni@C can be observed in selected-area electron diffraction (SAED) pattern (Fig. 1b inset), which may owe to the small size and few loading amount of the Ni@C [24,31]. Just as demonstrated in HR-TEM results, an intimate contact interface between the binary nanocomposites formed instead of a simple physical mixture of two components which is crucial for efficient charge transfer [32].

The phase structures of g-C_3N_4 and Ni@C/g-C_3N_4 samples were characterized by X-ray diffraction (XRD) (Fig. 2). At first glance, all of the specimens have the two typical diffraction peaks of g-C_3N_4 at 13.0° and 27.6°, indicating that the structure of g-C_3N_4 did not change after the immobilization of Ni@C, consistent with the results of SEM and TEM. And the characteristic ray peaks index to the (100) and (002) crystal planes of g-C_3N_4 corresponding to the periodic array of the in-planar tri-s-triazine unit and the stacking layered structure of aromatic rings, respectively [33]. Compared with pure g-C_3N_4, there is an evident peak situating at 22.4°, which can be ascribed to the graphitized carbon layers [24,34]. Meanwhile, no distinct peak of Ni was observed, implying that the sizes of Ni clusters are quite small in accordance with the SAED result [35]. Fourier transform infrared (FTIR) spectrophotometer spectra were employed to analyze the chemical structures of the photocatalysts (Fig. 3). Obviously, FTIR spectrums of the samples are similar indicating that the bulk structure and core chemical skeleton of g-C_3N_4 did not change after the modification with Ni@C. The broad peak between 3500 and 3000 cm^{-1} caused by the stretching vibration of N—H and O—H in the physically adsorbed water was observed. The

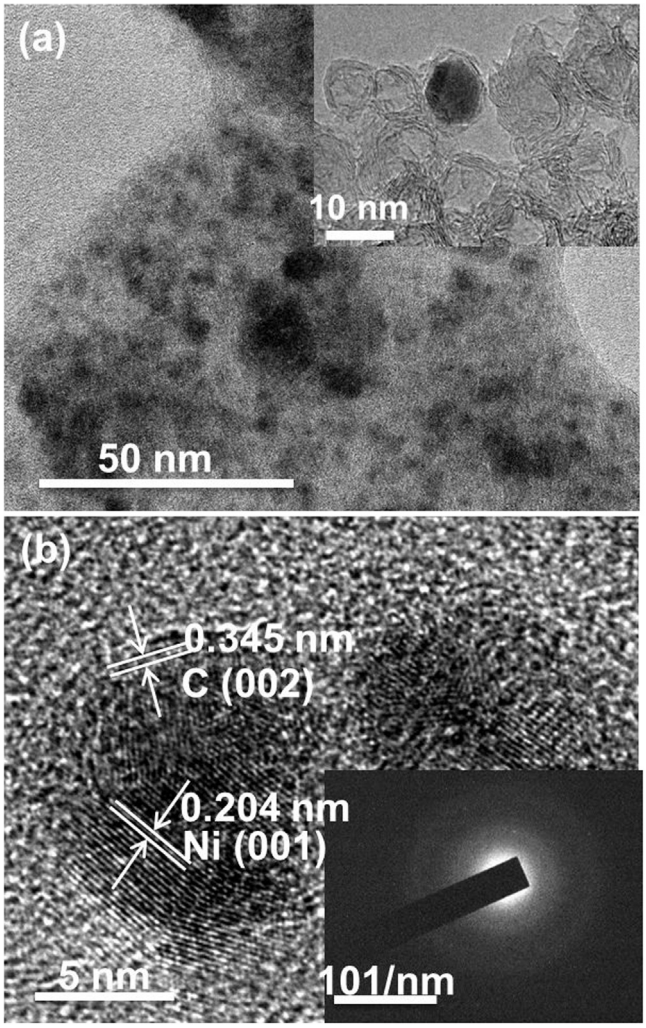

Fig. 1. (a) A magnified TEM image of 2.0 wt% Ni@C/g-C_3N_4. The inset displays the TEM image of Ni@C grains. (b) HR-TEM image of Ni@C embedded in g-C_3N_4. The inset displays the corresponding selected area electron diffraction (SAED) pattern of Ni@C co-catalyst.

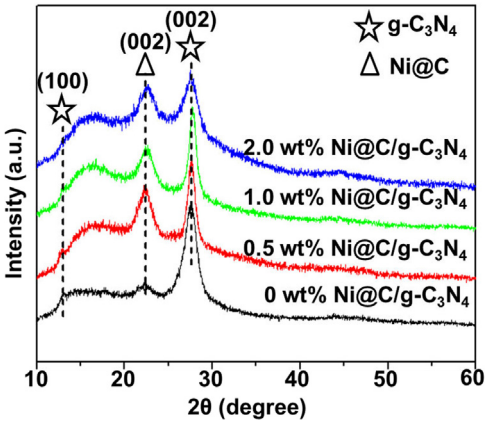

Fig. 2. XRD patterns of x wt% Ni@C/g-C_3N_4 (x = 0, 0.5, 1.0, 2.0).

set of peaks in the range of 1200 and 1700 cm^{-1} is attributed to the stretching vibration of CN heterocycles. The sharp peak at around 810 cm^{-1} is ascribed to the typical breathing vibration of triazine units [36]. In comparison with pure g-C_3N_4, the peaks shown some enhanced absorption and slight shift which may be caused by the

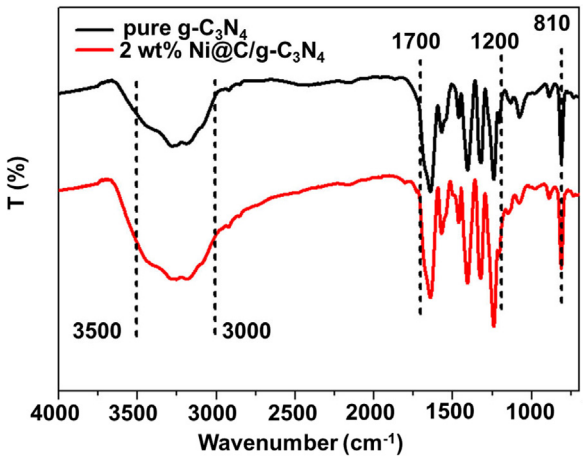

Fig. 3. FTIR spectra of pure g-C_3N_4 and 2.0 wt% Ni@C/g-C_3N_4.

presence of Ni@C on the surface of g-C_3N_4 [37]. The Raman spectra of the two samples further confirmed the existence of graphitic carbon structures in the Ni@C/g-C_3N_4 composites. Both of the two specimens have the typical bands of g-C_3N_4 at around 458, 693, 734, 964, 1217, and 1296 cm^{-1} (Fig. S3) [38]. Compared with pure g-C_3N_4, another two peaks of the composites can be observed that attributed to the typical disordered band (D band) and graphene band (G band) respectively [39]. According to the elemental analysis (EA) results (Table S1), the molar ratio of C to N for pristine g-C_3N_4 is 0.652, well agreeing with previous report [40]. After loading of 2.0 wt% Ni@C, the value increased to 0.683, indicating the existence of Ni@C co-catalyst in the photocatalysts.

The chemical composition and chemical states of surface elements of the as-prepared samples were probed by X-ray photoelectron spectroscopy (XPS) measurement. As expected, in addition to C, N and O, Ni element was also characterized by XPS. As can be seen from Fig. 4 and Fig. S6, both samples have the characteristic peaks of g-C_3N_4. The dominance peak of C 1s (284.6 eV) originated from the polluted carbon of (C-C), such as the carbon of surrounding environment [41]. The other peak situating at 287.9 eV can be ascribed to the sp^2-hybridized carbon in the N-containing aromatic ring (N=C—N) [41]. The N 1s XPS signal could be deconvoluted into three main peaks centering at 398.5 eV, 399.6 eV and 401.1 eV which could be attributed to sp^2-hybridized nitrogen in triazine rings (N=C—N), tertiary nitrogen N-$(C)_3$ groups and amino functions carrying hydrogen (C-N-H) respectively from lower to higher energy [42]. Moreover, there is an unconspicuous peak at 404.2 eV which can be assigned to the positive charge localization in heterocycles and this result agrees well with previously reported species data [43]. Meanwhile, it is obvious that the peaks position as well as the peaks intensity of C 1s and N 1s shown some difference after loading 2.0 wt% Ni@C. This indicates the strong chemical interaction (electron coupling) between the primary catalyst and the co-catalyst which gives a solid evidence that the interface between g-C_3N_4 and Ni@C is so close to facilitate the transfer of photo-generated electrons [40,44]. This maybe due to that both of the components have common carbon elements and the junctions between g-C_3N_4 and Ni@C could be readily formed [45]. Compared with pure g-C_3N_4, the new peak at around 285.3 eV could be attributed to carbon atoms bonded to nickel atoms (C-Ni) [46].

Ultraviolet–visible (UV–vis) diffuse reflectance spectroscopy analysis was used to investigate the synergetic effect of Ni@C and g-C_3N_4 on the light absorption properties demonstrated in Fig. 5.

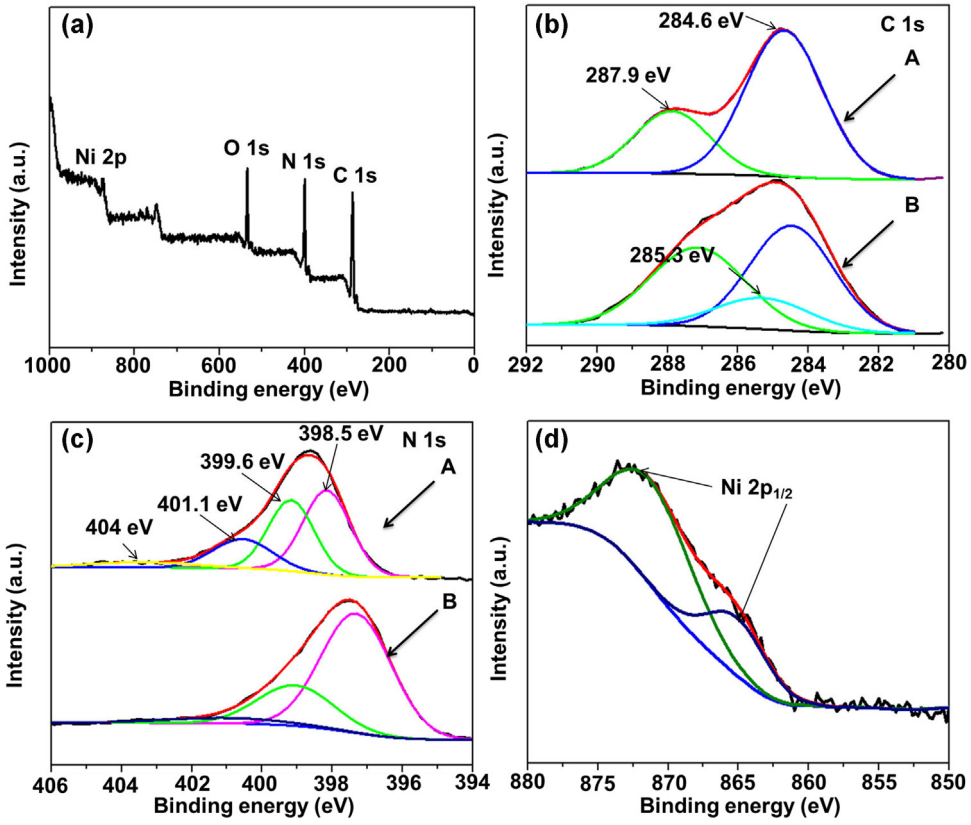

Fig. 4. (a) XPS spectrum of the 2.0 wt% Ni@C/g-C_3N_4 before irradiation. (b) C 1s and (c) N 1s XPS spectra of g-C_3N_4 before (A) and after (B) modification with Ni@C co-catalyst. (d) XPS spectrum of Ni 2p before catalytic reaction. All peaks were referenced to the adventitious carbon 1 s located at 284.6 eV.

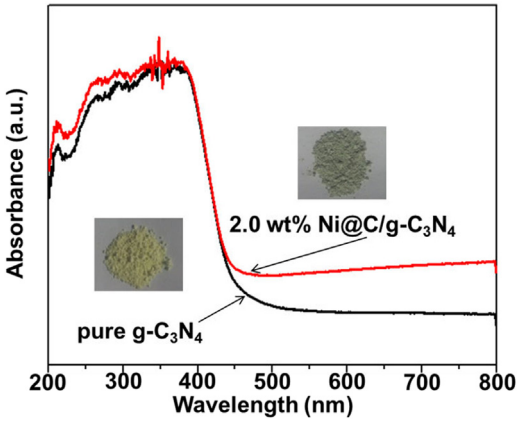

Fig. 5. UV–vis absorption spectra of pure g-C_3N_4 and 2.0 wt% Ni@C/g-C_3N_4. Inset: digital photos of the catalysts.

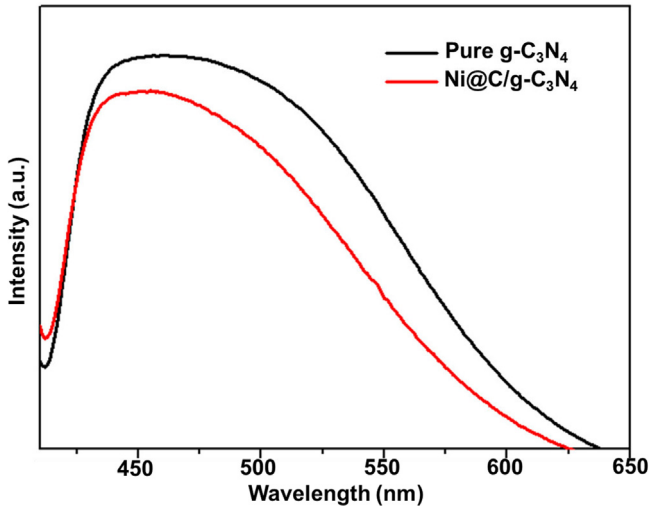

Fig. 6. PL spectra under 400 nm excitation for g-C_3N_4 and Ni@C/g-C_3N_4 samples.

Both of two samples showed the typical semiconductor absorption of g-C_3N_4 and exhibited the absorption edge at around 460 nm, corresponding to the optical band gap of 2.7 eV by a related curve of $(\alpha h\upsilon)^{1/2}$ *vs.* photon energy (Fig. S4) [40]. This indicates that Ni@C nanoparticles were not doped into the lattice of g-C_3N_4 while rather loaded on the surface of g-C_3N_4 [38]. Compared with pure g-C_3N_4, the introduction of Ni@C increased the absorption of visible range after 550 nm which was helpful for improving the photocatalytic efficiency. The increase of absorption in the visible light region can be attributed to the introduction of black body properties of Ni@C. Although the absorbed light by Ni@C cannot produce any active electrons or holes for photocatalytic reaction, they can be converted to heat, thereby creating a special photothermal effect on the photocatalyst surface which was beneficial for boosting the photoinduced electron-hole migration rate and thus enhancing the photocatalytic activity [47]. And a distinct color change from light yellow to gray is depicted in the inset of Fig. 5. In Fig. S5, the photocatalytic H_2 production has the similar trend with the optical absorption of the sample. It deserved to note that H_2 evolution was observed up to 550 nm, which corresponds to the absorption range of 2.0 wt% Ni@C/g-C_3N_4. The photoluminescence (PL) spectra of pure g-C_3N_4 and Ni@C/g-C_3N_4 excited by 400 nm light at room temperature were shown in Fig. 6. As we can see, the two samples exhibit broad emission peaks centering at around 450 nm. Obviously, the PL intensity of Ni@C/g-C_3N_4 is weaker than that of pure g-C_3N_4, suggesting that the recombination rate of the photo-

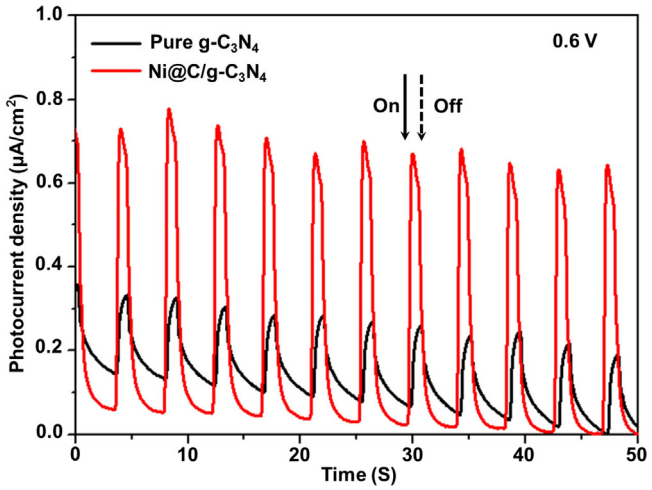

Fig. 7. Transient photocurrent generation from pure g-C_3N_4 and 2.0 wt% Ni@C/g-C_3N_4 electrodes at 0.6 V versus Ag/AgCl in 0.2 M Na_2SO_4 containing 10 vol.% TEOA under simulated sunlight irradiation in a standard three electrode photoelectrochemical cell.

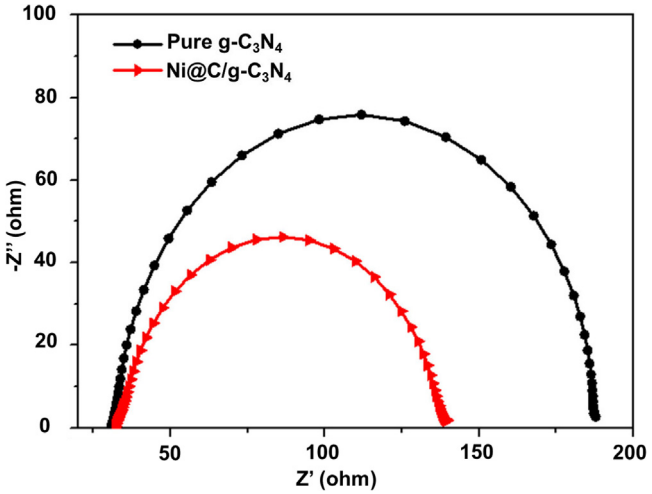

Fig. 8. Nyquist plots of EIS for pure g-C_3N_4 and 2.0 wt% Ni@C/g-C_3N_4 samples.

generated electron-hole pairs can be effectively suppressed after modified with Ni@C, and this may be originated from the help of co-catalyst trapping charge carriers [48].

Fig. 7 shows the transient photocurrent responses of pure g-C_3N_4 and 2.0 wt% Ni@C/g-C_3N_4 samples tested at a constant voltage of 0.6 V versus Ag/AgCl with several on-off cycles of intermittent simulated sunlight irradiation. Both of the two photoanodes demonstrated prompt photocurrent generation during the on and off cycles of illumination. The photocurrent intensity of 2.0 wt% Ni@C/g-C_3N_4 photoanode was more than three times higher than that of pure g-C_3N_4 photoanode. EIS measurements of the two samples were conducted under visible light illumination to study the interfacial charge transfer and recombination rates occurring in the three electrode systems (Fig. 8). It is obviously that the Nyquist plots of g-C_3N_4 have a much smaller semicircular after loading Ni@C, suggesting the positive roles of the co-catalyst in accelerating charge transport and separation.

The photocatalytic activity of the samples was tested through the amount of H_2 production from water splitting with triethanolamine (TEOA) as a sacrificial electron donor under visible-light irradiation. As can be seen from Fig. 9 and Fig. S7, the H_2 production rate increased with augmenting Ni@C content in the range of 0.5–2 wt%. And the generation rate within 2 h can

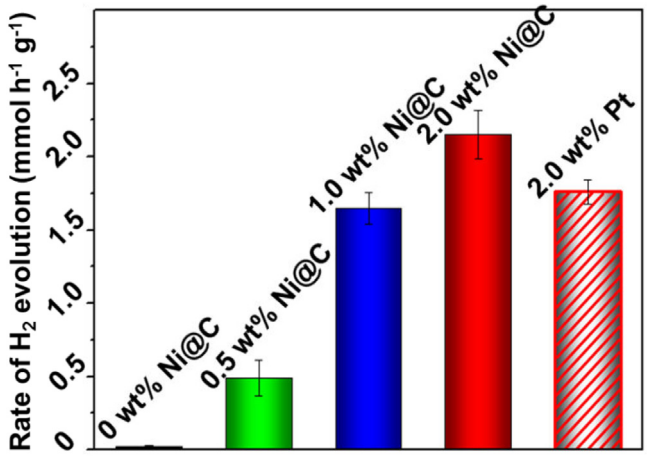

Fig. 9. H_2 evolution rates over x wt% Ni@C/g-C_3N_4 (x = 0, 0.5, 1.0, 2.0) and 2.0 wt% Pt/g-C_3N_4 within 2 h. All the experiments were conducted in 20 vol% TEOA aqueous solution at room temperature under visible light irradiation (λ > 420 nm). Error bars represent mean values and standard deviations of two independent experiments.

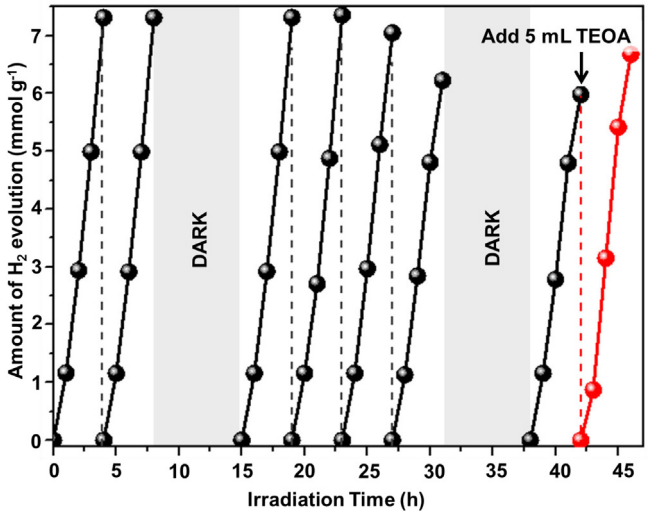

Fig. 10. The typical time course of H_2 production in aqueous triethanolamine solution (20 vol%) under visible light with 30 mg of 2.0 wt% Ni@C-deposited g-C_3N_4. The reaction was continued for 46 h with three intermediate evacuations.

reach 2.15 mmol h^{-1} g^{-1} for the optimum Ni@C/g-C_3N_4 (Ni@C:g-C_3N_4 = 2 wt%) which was much better than that of pure g-C_3N_4, here by about a factor of 88 with a 2.14% apparent quantum efficiency at 420 nm. Furthermore, the rate was even higher than that of 2.0 wt% Pt/g-C_3N_4. The results imply that Ni@C can function as an effective "precious-metal-free" co-catalyst for visible-light-driven H_2 production. A long-term photostability is crucial for photocatalysts practical application. As displayed in Fig. 10, the reaction proceeded for a total of 46 h with eight recycle tests to measure the stability of 2.0 wt% Ni@C/g-C_3N_4 under visible-light irradiation (λ > 420 nm). The photostability of the given photocatalyst is superior to those reported previously suggesting that the strategy encapsulating metallic Ni in graphene layers offers a method to prevent the corrosion of the reactive center from taking place [49–51]. When the irradiation time extended to more than 20 h, the H_2 production rate start to fall slightly which may be caused by the oxidization of Ni cores or the consumption of sacrificial agent. Comparing Fig. 4d and Fig. S6, there is a slight difference between initial and after catalytic reaction for Ni XPS peaks. As shown in Fig. 4d, no signal in the range of 850 eV and 860 eV could be detected, implying that metallic Ni cores were protected well

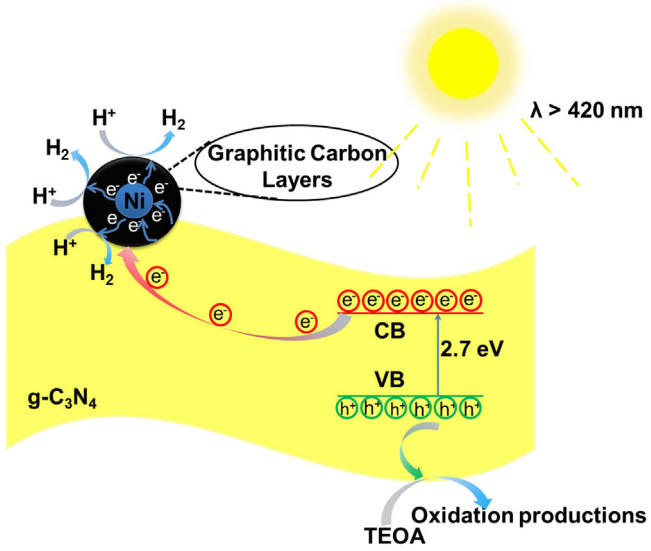

Fig. 11. Photocatalytic reaction mechanism of H_2 evolution reaction on Ni@C/g-C_3N_4.

by the graphene carbon shells and this is identical with previous reports [46,52]. Besides, the plasma atomic emission spectroscopy (ICP) analysis demonstrated that the Ni content in the photocatalyst declined from 1.525 wt% to 0.444 wt% after 50 h illumination. The loss of Ni metal from the co-catalyst was another reason for deactivation. Before the eighth recycle test, 5 mL TEOA was added into the reaction system and the H_2 generation rate arised slightly. On the basis of above analysis, a reaction mechanism on this photocatalyst can be proposed (Fig. 11). Under the irradiation of visible-light (λ > 420 nm), most of the photo-generated electrons can be trapped by metallic Ni nanoparticles, which was wrapped up by graphitized carbon materials. Meanwhile, holes were consumed by sacrifice reagent, which suppresses the recombination of the electrons and holes. H_2 evolution reactions occur on the surfaces of graphene layers that can restrain the formation metal-H_2 bonds. Additionally, the hollow onion-like structure may inhibit the undesirable reverse reaction from taking place.

4. Conclusion

In summary, the efficient and affordable photocatalyst, Ni@C/g-C_3N_4 was successfully prepared by facile wet impregnation method. Under optimal conditions, the H_2 generation rate could reach 2.15 mmol h^{-1} g^{-1} which was 88 times higher than that of pure g-C_3N_4 under visible light irradiation (λ > 420 nm). The outstanding performance can be attributed to the noble-metal-free co-catalyst, Ni@C, obtained by carbonization of MOFs and HCl treatment. The hollow onion-like structure endows the co-catalyst with many excellent properties, such as enhance the electronic conductivity, suppression the reverse reaction. To some extent, Ni metal can be protected from being corroded under the shield of graphene layers. We anticipate this work may open up new insights to improve the photocatalytic conversion efficiency by architecturally designing new co-catalysts.

Acknowledgements

This work was financially supported by National Natural Science Foundation of China (21573068), SRF for ROCS, SEM, SRFDP, Program of Shanghai Subject Chief Scientist (15XD1501300), Fundamental Research Funds for the Central Universities (WD1313009

and WD1514303), China Postdoctoral Science Foundation Funded Project (2016M591615) and 111 Project (B14018).

Appendix A. Supplementary data

Supplementary data associated with this article can be found, in the online version, at http://dx.doi.org/10.1016/j.apcatb.2016.07.033.

References

[1] A. Fujishima, K. Honda, Nature 238 (1972) 37–38.
[2] A. Kudo, Y. Miseki, Chem. Soc. Rev. 38 (2009) 253–278.
[3] L. Liao, Q.H. Zhang, Z.H. Su, Z.Z. Zhao, Y.N. Wang, Y. Li, X.X. Lu, D.D. Wei, G.Y. Feng, Q.K. Yu, X.J. Cai, J.M. Zhao, Z.F. Ren, H. Fang, F. Robles-Hernandez, S. Baldelli, J.M. Bao, Nat. Nanotechnol. 9 (2014) 69–73.
[4] X.C. Wang, K. Maeda, A. Thomas, K. Takanabe, G. Xin, J.M. Carlsson, K. Domen, M. Antonietti, Nat. Mater. 8 (2009) 76–80.
[5] J.P. Zou, L.C. Wang, J.M. Luo, Y.C. Nie, Q.J. Xing, X.B. Luo, H.M. Du, S.L. Luo, S.L. Suib, Appl. Catal. B: Environ. 193 (2016) 103–109.
[6] F. Dong, Y.H. Li, Z.Y. Wang, W.K. Ho, Appl. Surf. Sci. 358 (2015) 393–403.
[7] J.S. Zhang, M.W. Zhang, C. Yang, X.C. Wang, Adv. Mater. 26 (2014) 4121–4126.
[8] G. Liu, P. Niu, C. Sun, S.C. Smith, Z. Chen, G.Q. Lu, H.M. Cheng, J. Am. Chem. Soc. 132 (2010) 11642–11648.
[9] J. Liu, Y. Liu, N. Liu, Y. Han, X. Zhang, H. Huang, Y. Lifshitz, S.-T. Lee, J. Zhong, Z.H. Kang, Science 347 (2015) 970–974.
[10] J.R. Ran, T.Y. Ma, G.P. Gao, X.-W. Duc, S.Z. Qiao, Energy Environ. Sci. 8 (2015) 3708–3717.
[11] M.W. Zhang, X.C. Wang, Energy Environ. Sci. 7 (2014) 1902–1906.
[12] P. Niu, L.-C. Yin, Y.-Q. Yang, G. Liu, H.-M. Cheng, Adv. Mater. 26 (2014) 8046–8052.
[13] C. Ye, J.-X. Li, Z.-J. Li, X.-B. Li, X.-B. Fan, L.-P. Zhang, B. Chen, C.-H. Tung, L.-Z. Wu, ACS Catal. 5 (2015) 6973–6979.
[14] J.H. Yang, D. Wang, H.X. Han, C. Li, Acc. Chem. Res. 46 (2013) 1900–1909.
[15] Q.H. Liang, Z. Li, Z.-H. Huang, F.Y. Kang, Q.-H. Yang, Adv. Funct. Mater. 25 (2015) 6885–6892.
[16] G.G. Zhang, S.H. Zang, X.C. Wang, ACS Catal. 5 (2015) 941–947.
[17] C.C. Hu, H.S. Teng, J. Catal. 272 (2010) 1–8.
[18] Y. Xu, R. Xu, Appl. Surf. Sci. 351 (2015) 779–793.
[19] A. Indra, P.W. Menezes, K. Kailasam, D. Hollmann, M. Schröder, A. Thomas, A. Brücknerc, M. Driess, Chem. Commun. 52 (2016) 104–107.
[20] Q.D. Yue, Y.Y. Wan, Z.J. Sun, X.J. Wu, Y.P. Yuan, P.W. Du, J. Mater. Chem. A 3 (2015) 16941–16947.
[21] S.J. Yang, T. Kim, J.H. Im, Y.S. Kim, K. Lee, H. Jung, C.R. Park, Chem. Mater. 24 (2012) 464–470.
[22] Q. Liu, Y.R. Guo, Z.H. Chen, Z.G. Zhang, X.M. Fang, Appl. Catal. B: Environ. 183 (2016) 231–241.
[23] W. Xia, A. Mahmood, R. Zou, Q. Xu, Energy Environ. Sci. 8 (2015) 1837–1866.
[24] L.L. Fan, P.F. Liu, X.C. Yan, L. Gu, Z.Z. Yang, H.G. Yang, S.L. Qiu, X.D. Yao, Nat. Commun. 7 (2016) 10667.
[25] C.X. Zhao, H. Luo, F. Chen, P. Zhang, L.H. Yic, K.Y. You, Energy Environ. Sci. 7 (2014) 1700–1707.
[26] L.X. Zhang, Q.L. Liu, T. Aoki, P.A. Crozier, J. Phys. Chem. C 119 (2015) 7207–7214.
[27] K.S. Novoselov, V.I. Fal'ko, L. Colombo, P.R. Gellert, M.G. Schwab, K. Kim, Nature 490 (2012) 192–200.
[28] B. Chai, T.Y. Peng, J. Mao, K. Lia, L. Zan, Phys. Chem. Chem. Phys. 14 (2012) 16745–16752.
[29] J. Xing, H.B. Jiang, J.F. Chen, Y.H. Li, L. Wu, S. Yang, L.R. Zheng, H.F. Wang, P. Hu, H.J. Zhao, H.G. Yang, J. Mater. Chem. A 1 (2013) 15258–15264.
[30] S. Cao, J.X. Low, J.G. Yu, M. Jaroniec, Adv. Mater. 27 (2015) 2150–2176.
[31] Y.H. Li, J. Xing, Z.J. Chen, Z. Li, F. Tian, L.R. Zheng, H.F. Wang, P. Hu, H.J. Zhao, H.G. Yang, Nat. Commun. 4 (2013) 2500.
[32] S. Cao, Y. Chen, L. Kang, Z.S. Lin, W.-F. Fu, J. Mater. Chem. A 3 (2015) 18711–18717.
[33] F. Dong, L.W. Wu, Y.J. Sun, M. Fu, Z.B. Wu, S.C. Lee, J. Mater. Chem. 21 (2011) 15171–15174.
[34] Y.H. Qu, Z. Zhang, X.W. Wang, Y.Q. Lai, Y.X. Liua, J. Li, J. Mater. Chem. A 1 (2013) 14306–14310.
[35] Y.R. Fan, X.J. Li, X.C. He, C.M. Zeng, G.Y. Fan, Q.Q. Liu, D.M. Tang, Int. J. Hydrogen Energy 39 (2014) 19982–19989.
[36] W.-J. Ong, L.-L. Tan, S.-P. Chai, S.-T. Yong, Chem. Commun. 51 (2015) 858–861.
[37] C.B. Li, Z.J. Li, S. Yu, G.X. Wang, F. Wang, Q.Y. Meng, B. Chen, K. Feng, C.H. Tung, L. Wu, Energy Environ. Sci. 6 (2013) 2597–2602.
[38] Q.J. Xiang, J.G. Yu, M. Jaroniec, J. Phys. Chem. C 115 (2011) 7355–7363.
[39] Y.Y. Wen, H.M. Ding, Y.K. Shan, Nanoscale 3 (2011) 4411–4417.
[40] Y.D. Hou, A.B. Laursen, J.S. Zhang, G.G. Zhang, Y.S. Zhu, X.C. Wang, S. Dahl, I. Chorkendorff, Angew. Chem. Int. Ed. 52 (2013) 3621–3625.
[41] X.X. Xu, G. Liu, C. Randorn, J.S. Irvine, Int. J. Hydrogen Energy 36 (2011) 13501–13507.
[42] Y.G. Li, R.R. Wang, H.J. Li, X.L. Wei, J. Feng, K.Q. Liu, Y.Q. Dang, A. Zhou, J. Phys. Chem. C 119 (2015) 20283–20292.
[43] A. Thomas, A. Fischer, F. Goettmann, M. Antonietti, J.-O. Müller, R. Schloögl, J.M. Carlsson, J. Mater. Chem. 18 (2008) 4893–4908.
[44] B. Chai, T.Y. Peng, J. Mao, K. Li, Ling Zan, Phys. Chem. Chem. Phys. 14 (2012) 16745–16752.
[45] K. Chang, X. Hai, J.H. Ye, Adv. Energy Mater. (2016), http://dx.doi.org/10.1002/aenm.201502555.
[46] J.Y. Liu, C.S. Zhuang, K. Li, T.Y. Peng, Phys. Chem. Chem. Phys. 17 (2015) 10944–10952.
[47] J.X. Low, B. Cheng, J.G. Yu, M. Jaroniec, Energy Storage Mater. 3 (2016) 24–35.
[48] M.Y. Ding, W. Wang, Y.J. Zhou, C.H. Lu, Y.R. Ni, Z.Z. Xu, J. Alloys Compd. 635 (2015) 34–40.
[49] J.L. Yuan, J.Q. Wen, Y.M. Zhong, X. Li, Y.P. Fang, S.S. Zhang, W. Liu, J. Mater. Chem. A 3 (2015) 16941–16947.
[50] T. Zhu, H.B. Wu, Y.B. Wang, R. Xu, X.W. Lou, Adv. Energy Mater. 2 (2012) 1497–1502.
[51] J. Deng, P.J. Ren, D.H. Deng, X.H. Bao, Angew. Chem. Int. Ed. 54 (2015) 2100–2104.
[52] T.Y. Peng, X.H. Zhang, P. Zeng, K. Li, X.G. Zhang, X.G. Li, J. Catal. 303 (2013) 156–163.